Measurement 50 (2014) 135–140

Contents lists available at ScienceDirect

Measurement

journal homepage: www.elsevier.com/locate/measurement

Detection limits for glow discharge mass spectrometry (GDMS) analyses of impurities in solar cell silicon

Marisa Di Sabatino *

Department of Materials Science and Engineering, Norwegian University of Science and Technology (NTNU), 7491 Trondheim, Norway

ARTICLE INFO

Article history:
Received 7 March 2013
Received in revised form 18 December 2013
Accepted 23 December 2013
Available online 4 January 2014

Keywords:
Silicon
Impurities
Glow discharge
Mass spectrometry
Solar cells

ABSTRACT

The measurement of both doping elements and trace elements in solar cell silicon plays a key role for achieving high conversion efficiency of the solar cell device. Doping element concentrations in the range of few hundreds part per billions (ppb) and trace elements in the ppb or sub-ppb concentration range are typically present in multicrystalline silicon wafers for solar cells. Accurate and reliable measurements of these small amounts are not straightforward. The present work describes a fast-flow direct-current high resolution glow discharge mass spectrometer (GDMS). Detection limits for a number of impurities (B, Al, P, Ca, Ti, V, Cr, Mn, Fe, Ni, Co, Cu, Mo, Sn, W and Pb) of interest for solar cell applications have been investigated by GDMS. These detection limits are approximately 1 ppba or below, except for B, Al, P, Ca and Pb. All concentrations reported are quantitative since calculated relative sensitivity factors (RSF's) for Si matrix have been used. The detection limits have been achieved with minimum sample preparation and short analysis time.

1. Introduction

Impurities in trace amounts degrade the properties of silicon for solar cell applications. They are mainly introduced by the feedstock material, crucible, coating, furnace components and atmosphere. Transition elements are typically present in tens to thousand of ppba in the silicon feedstock. Multicrystalline (mc) silicon solar cells are made from directional solidified ingots and, due to segregation, the level of most of the impurities in the final mc-Si wafers (prior to solar cell processing) is less then tens of ppba. Dissolved transition elements introduce deep levels in the band gap thus increasing the carrier recombination rate. For some common impurity elements, e.g., iron, chromium and titanium, this effect is significant at concentrations on the order of a few ppba [1–6]. Davis et al. [1] studied several impurities in single-crystalline (sc) silicon made by the Czochralski process and reported on their effect on solar cell efficiency. According to their investigation, the addition of 1 ppba Ti or 140 ppba Fe or 100 ppba Cr to the silicon wafers causes 30% decrease of the normalized solar cell efficiency. Istratov et al. [7] and Macdonald et al. [8] reported on the typical levels of impurities in mc-Si wafers and showed that the levels of Fe, Cr, Cu, Ni and Co range between 3×10^{12} to 3×10^{14} cm^{-3} (approximately 0.1-10 ppba). Coletti [9] reported on the effect of Fe, Cr, Ni and Ti on multicrystalline silicon solar cells. Recently, the level of impurities in the so-called solar-grade silicon (SoG-Si) feedstock has been the focus of many investigations [4,10,11]. It was shown [11] that a SoG-Si feedstock containing 83 ppba Al and 99 ppba Ti will give a 3% relative reduction of solar cell efficiency. Specifications for SoG-Si feedstock are currently under discussion. The main attention is given to the concentration of doping elements, e.g. B and P, since they are more difficult to remove during directional solidification and since they directly affect the solar cell base resistivity. Typical levels of B and P in undoped SoG feedstock materials are <130 ppba and <90 ppba, respectively [9].

Being able to measure, hence control, the concentration of both the doping elements and trace elements in solar

* Tel.: +47 98243462.
E-mail address: Marisa.di.sabatino@material.ntnu.no

0263-2241/$ - see front matter © 2014 Published by Elsevier Ltd.
http://dx.doi.org/10.1016/j.measurement.2013.12.024

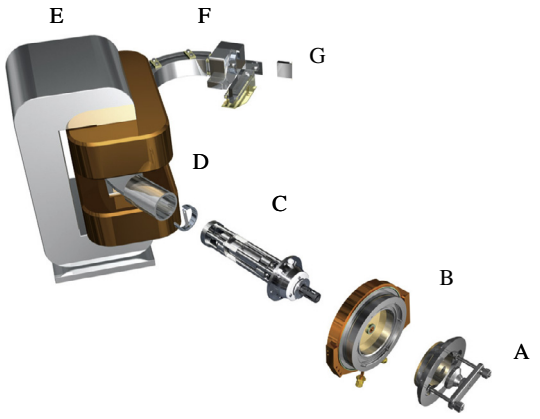

Fig. 1. GDMS main components: A – sample holder; B – plasma chamber; C – ion optic assembly; D – resolution slit; E- magnet; F – electro-static analyser; G – detector. (Courtesy Thermo Fisher).

cell silicon play a key role for achieving the highest energy conversion efficiency of the devices. However, as indicated above, these amounts are quite low. Therefore, accurate and reliable measurements of these materials are not straightforward. The techniques to analyze transition elements in the ppba level in silicon include neutron activation analysis (NAA), micro X-ray fluorescence spectroscopy (μ-XRF), glow discharge mass spectrometry (GDMS), secondary ion mass spectrometry (SIMS) and, to a certain extent, also inductively coupled plasma mass spectrometry ICP-MS. However, in terms of sensitivity and quantification capabilities as well as easy to perform the analysis in a relatively short time, the GDMS instruments are superior to analyse conducting and semiconducting samples in the low ppb range compared to the other techniques. Currently, the GDMS instruments are receiving increasing attention for the analyses of materials for photovoltaic (PV) applications [12,13]. However, no data have been reported for the limits of the detection and capability of these instruments. Therefore, in the present work the determination of detection limits of GDMS analyses for several elements of interest in PV silicon are described and discussed in details.

2. Experimental

2.1. The GDMS instrument

The instrument used in this study is a fast-flow direct-current high resolution glow discharge mass spectrometer (GDMS). Fig. 1 shows the main components of the GDMS [14,15]. In this type of instruments, the sample forms a cathode in a low pressure gas discharge, Argon in this study. The glow discharge ion source is a Grimm-type, which allows for both surface and in-depth analysis by controlling the discharge parameters to obtain planar sputtering [16]. The samples must have a flat and smooth surface, and are loaded in the sample holder. Ions generated in the plasma chamber are focussed by the ion optic assembly onto the resolution slit before entering the magnet. After the mass separation by the ions' momentum in the magnetic field, the electro-static analyser (ESA) serves for an energy separation to achieve high resolution capabilities required for separation of polyatomic interference species from the analyte signals. Finally the ions on their respective masses are counted by the detection system. Different kinds of ionization processes occur in the plasma chamber as indicated in Fig. 2. The Element GD has three detector modes, namely the counting and analog detector obtained from a secondary electron multiplier (SEM), and the Faraday detector. The resolution slit allows choosing between low ($R = 400$), medium ($R = 4000$) and high ($R = 10{,}000$) resolutions (i.e. $m/\Delta m$). Due to the ratio of the mass of each element over its charge, m/Z, the ions are separated by the analyzer.

2.2. Quantification

The intensity of the element signal relative to the matrix signal allows quantification of the concentration of each element. When trace elemental analyses are performed on high purity materials, such as in this study, the ion signal for the matrix (I_M) is assumed to be large relative to the individual elements (I_X). Therefore, the matrix ion current is a good approximation of the total ion current, and the matrix can be assumed to have concentration of 100%. The concentration K of an element X, K_X, can be calculated as [17]:

$$K_X = \left(\frac{I_X}{I_M}\right) K_M \left(\frac{A_M}{A_X}\right) \quad (1)$$

where K_X and K_M are the atomic mass fraction of the element and matrix, respectively; I_X and I_M are the ion beam signals of the element and matrix, respectively; A_X and A_M are the isotope abundances of the element and matrix, respectively.

In order to obtain quantitative results, a concentration dependence of element-specific and matrix-specific sensitivity factors (named relative sensitivity factors, RSF's) has to be known. The element concentration in mass unit, C_X, can be expressed as:

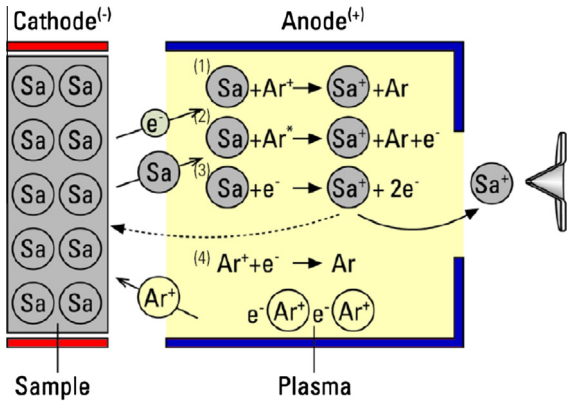

Fig. 2. Schematic view of the plasma chamber with the sample (cathode) on the left and the cone on the right. (1) to (4) are the ionization processes occurring in the chamber (Courtesy Thermo Fisher).

$$C_X = K_X RSF_X \quad (2)$$

where K_X is the uncorrected apparent element concentration (Eq. (1)) and RSF_X is the relative sensitivity factor of the element X in the matrix.

The RSF's depend on the factors that influence ion intensities, such as sample matrix, atomization source, sampling and detection conditions [17,18]. Recently, RSF's have been calculated for Si matrices [17] and are reported in Table 1 for the conditions used in this study (i.e. 60 mA, 300 ml/min and 1000 V).

2.3. Samples and samples preparation

Two 20 × 30 × 10 mm monocrystalline silicon samples produced by the Czochralski (CZ) process were selected for this investigation. The two samples were p- and n-type silicon with resistivities of 1.7 Ω cm and 10.7 Ω cm, respectively. These samples were selected from the middle of two CZ ingots. The ingots were grown from electronic-grade silicon (EG-Si) feedstock and have, therefore, high purity. Thus it was expected that, except the two doping elements (B in the p-type ingot and P in the n-type ingot), all transition metallic impurities will not be detected. Therefore, the quantification of the peaks corresponds to the noise level for each element position.

All samples were ground to 500 grid SiC-paper, and carefully cleaned with de-ionised water and ethanol, and dried. The sputter rate for Si matrices is approximately 20 nm/s. The instrument has a lateral resolution of 8 mm and a depth resolution on the order of 10–1000 nm, depending on concentration level and number of the elements to be analysed. Prior to start of the analysis of the two CZ samples, a standard silicon sample with known chemistry (Si cast with addition of several elements in the ppb to ppm range) was analysed in order to centre the peaks. Thereafter, a "blank", i.e. a very pure silicon sample (no presence of trace elements), was used to clean the instrument. Both samples were prepared in the same way and analysed with the same conditions as the two CZ samples.

Table 1
RSF values for Si matrices (set 1 analysis parameters: 60 mA, 300 ml/min and 1000 V) with relative standard deviation (%) [17].

Element	RSF (set 1) (%)
B	1.5 ± 20
Al	0.8 ± 33
P	1.1 ± 31
Ca	0.4 ± 5
Ti	0.2 ± 6
V	0.2 ± 7
Cr	0.5 ± 16
Mn	0.3 ± 13
Fe	0.5 ± 14
Ni	0.4 ± 13
Cu	0.7 ± 20
Zn	0.1 ± 1
Mo	0.3 ± 3
Sn	0.3 ± 5
W	0.2 ± 2
Pb	0.2 ± 6

The p-type CZ sample was also analysed by a secondary ion mass spectrometry (SIMS) to assess the precision of the GDMS measurements. In this sample, only B concentration was compared. The instrument used is a Cameca IMS 7f magnetic sector SIMS. The source was operated at standard conditions with 10 keV O_2^+ as primary ions, and a raster size ranging from 100 to 200 μm.

2.4. Methodology

For each sample, three spots were analysed and each spot was pre-sputtered for 10 min. Each spot analysis was repeated five times and the last (fifth) analysis was used for the calculations. Thus six analyses were averaged in total for the two samples (three analyses per sample). The determination of the detection limits (or limits of detection, LoD) was calculated according to the following procedure:

- Since all elements are below the detection limits, a quantification of the background noise for each peak position is made.
- Average of six analyses (background noise) for all elements (except for B, in the p-type sample, and P, in the n-type samples) as in Eq. (3).
- Calculation of the standard deviation in the mean value for all elements as in Eq. (5).
- Calculation of the detection limits (LoD) as three times the standard deviation as in Eq. (6). This method is similar to the one used by Hinrichs et al. [19] and the confidence interval is 99.7%.

$$\bar{x} = \frac{1}{n}\sum_{i=1}^{n} C_{x_i} \quad (3)$$

$$STDV = \sqrt{\frac{1}{(n-1)}\sum_{i=1}^{n}(C_{xi} - \bar{x})^2} \quad (4)$$

$$\sigma_m = \frac{STDV}{\sqrt{n}} \quad (5)$$

where $\bar{x}$ is the average of all measurements for each element or isotope; C_{Xi} is the measured concentration C_X ("x" indicate one element or isotope) as defined in Eq. (2), for "i" number of measurements. STDV and σ_m indicate the standard deviation of the distribution of the single measurements and the standard deviation in the mean value, respectively; n is the number of measurements (in this study n is 6 for all elements, except B and P where n is 3).

$$LoD = 3\sigma_m \quad (6)$$

where LoD is the limit of detection.

The total analysis time for each spot (in this study a total of three spots, analysed five times each for both samples made investigated) was approximately 40 min (i.e. 6 × 5 min plus 10 min pre-sputtering). The depth of the crater for each analysis was not measured but it was expected to be quite homogeneous and flat, as also shown

Table 2
Analysis parameters and components materials.

Discharge current, DC: 60 mA
Discharge gas, DG: 300 ml/min (Ar)
Discharge voltage, DV: 1000 V
Matrix sensitivity: 1×10^{10} cps (medium resolution)
Anode material: steel; anode cup and flow tube: graphite; cone: steel

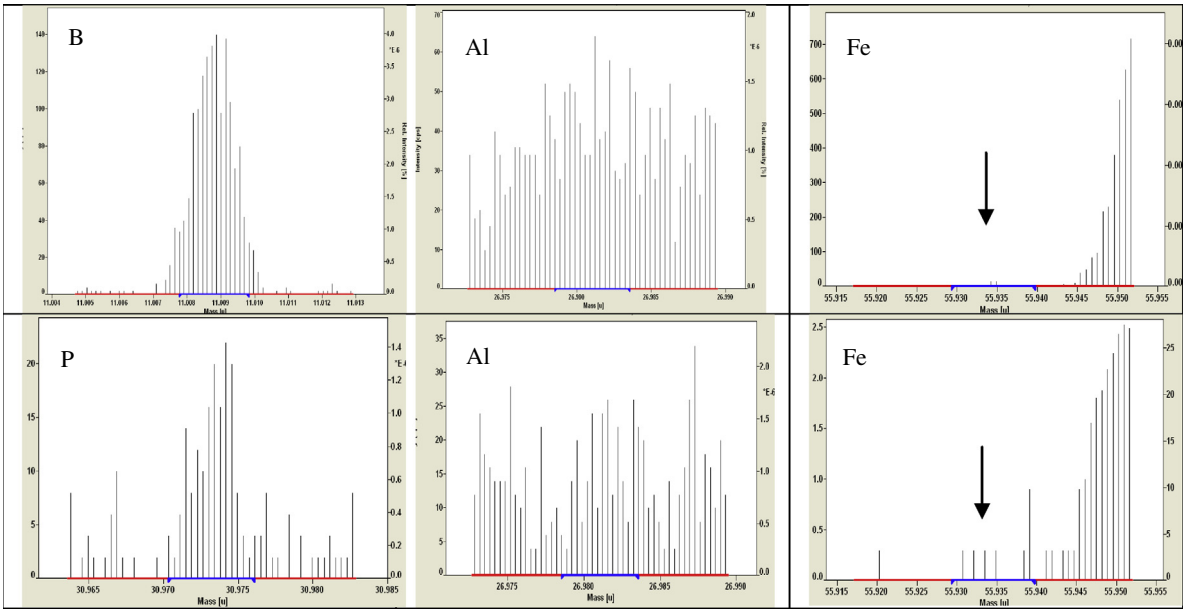

Fig. 3. GDMS spectra (intensity vs mass range) for three elements in the p-type (above) and n-type (below) samples.

in a recent work [20]. The total depth of each crater should be approximately 48 μm.

2.5. Analysis parameters

A prerequisite for achieving low detection limits, is a high signal-to-noise ratio. Therefore, the instrument was optimized to give the highest sensitivity for the silicon matrix signal. Prior to the analysis, the discharge current (DC), discharge gas (DG) and discharge voltage (DV) were adjusted to obtain the optimum signal intensity for the silicon matrix (i.e. intensity of the Si peak $\approx 1 \times 10^{10}$ cps). The achievable detection limits mainly depend on the signal-to-noise ratio of the analyzer used; since the background noise is constantly very low (<1 cps), detection limits are mostly influenced by obtaining a high matrix signal. Thus, having an intensity of the Si peak $\approx 1 \times 10^{10}$ cps will allow us to detect a noise or background <0.1 ppb. The cleanliness of the source parts used is another important parameter, thus high purity materials for the parts in direct contact with the glow discharge were used. The analysis parameters and components materials are given in Table 2. The elements analysed were: B, Al, P, Ca, Ti, V, Cr, Mn, Fe, Ni, Co, Cu, Mo, Sn, W and Pb. All elements were analysed in medium resolution ($R = 4000$).

3. Results and discussion

The GDMS spectra of the analysed samples are shown in Fig. 3. Three elements are selected in Fig. 3 to show the main doping element (B in p-type and P in n-type samples, respectively), aluminium and iron. Note that B and P peaks are element peaks, while the Al and Fe spectra show the noise level for these two elements. The high peak on the right-hand side of Fe is due to interferences ($^{28}Si^{28}Si$ and $^{40}Ar^{16}O$) while the area corresponding to the Fe peak is indicated by an arrow (Fig. 3). Table 3 reports all the measurements used in the calculations of the LoD (total of six spots except for B and P) as well as the average and standard deviation in the mean. Table 4 shows the limits of detection (LoD) calculated as three times the standard deviation in the mean value (Eq. (6)) of the GDMS measurements. Note that all results were calculated using Eq. (2) and the RSF values given in Table 1. Since the RSF value for cobalt was not known (not present in Table 1), 0.5 was used for Co (i.e. same RSF value as for Fe since they have similar atomic number). The results show that for most of the elements studied here the limit of detection is around 1 ppba. The LoD values for B, Al, P, Ca and Pb are above 1 ppba. The high value for Ca is probably due to the low abundance of the Ca isotope used, i.e. ^{44}Ca has

Table 3
All measurements (ppbw) included in the calculations of the LoD as well as the average and standard deviation in the mean (σ_m).

Element	Spot 1	2	3	4	5	6	Average	σ_m
B	0	0	1.5	–	–	–	0.5	0.7
Al	0	4.0	3.3	0	1.9	2.1	1.9	1.5
P	–	–	–	0	1.5	2.9	1.5	1.2
Ca	20.4	37.9	36.2	25.2	22.5	35.9	29.7	7.1
Ti	0	0	0.2	0.1	0.1	0.1	0.1	0.1
V	0.1	0.2	0.2	0.1	0.1	0.1	0.1	0.1
Cr	0.5	0.4	0.7	0.5	0.9	0.3	0.6	0.2
Mn	0.2	0.2	0.2	0.2	0.1	0	0.2	0.1
Fe	0	0	0.6	0	0.6	0	0.2	0.3
Ni	0	0	0.4	0.2	0.6	0.3	0.3	0.2
Co	0.2	0.2	0.2	0.2	0.2	0.2	0.2	0.03
Cu	0	0	1.1	0	1.1	0	0.4	0.5
Mo	0.6	0	0.8	1.1	0.5	0.2	0.5	0.4
Sn	0.5	0.4	0.5	0.5	0.3	0.4	0.4	0.1
W	0.2	0.2	0.7	0.3	0.2	0.1	0.3	0.2
Pb	0	1.1	2.5	1.8	1.0	0.7	1.2	0.8

Table 4
Limits of detection in mass (ppbw) and atomic concentrations (ppba).

Element	LoD, ppbw	LoD, ppba
B	2.1	5.3
Al	4.5	4.7
P	3.5	3.2
Ca	21.4	15.0
Ti	0.2	0.1
V	0.2	0.1
Cr	0.7	0.4
Mn	0.2	0.1
Fe	0.9	0.5
Ni	0.6	0.3
Co	0.1	0.05
Cu	1.6	0.7
Mo	1.1	0.3
Sn	0.3	0.1
W	0.5	0.1
Pb	2.4	0.3

approximately 2% abundance compared to ^{40}Ca which is approximately 97%. ^{40}Ca could not be used due to the presence of ^{40}Ar as the discharge gas, and thus a high interference in the mass spectrum. The confidence interval of the values in Table 4 is 99.7% since we have used $3 \times \sigma_m$ (Eq. (6). As a general rule, the precision obtained for each sample analysis depends on the count rate and counting time of each isotope. To improve the precision, and thus decrease the detection limits, longer counting times can be used, especially for important elements in Si (e.g. B, P, Al and Fe), and isotopes with low abundances (e.g. ^{44}Ca).

The results reported in Table 4 agree reasonable well with the values reported by Thermo Fisher Scientific for silicon matrices [19], being 1 ppba or below for most elements studied. However, they reported LoD of approximately 2.0 ppba for Ca, which is significantly lower than the value found in this study. Note that the values reported by Thermo Fisher Scientific [19] were only semi-quantitative since they applied standard RSF values (not calibrated for Si matrices). The detection limits reported in Table 4 can be further improved by changing the materials of the cone (Fig. 2) to reduce background signals, e.g. using cones made from graphite, and increasing the signal-to-noise ratio (background noise versus matrix sensitivity), e.g. increasing the counting times. Among the elements analysed, B and P might show high background due to possible contamination from the graphite parts. The use of graphite component with pyrolytically coated carbon (PyC) may help reducing the background.

The measured B concentrations on the same sample (p-type) using GDMS and SIMS were 1.7×10^{16} cm^{-3} and 1.8×10^{16} cm^{-3}, respectively, indicating that GDMS and SIMS show good agreement (approximately 6% difference). This also confirms the good precision of the GDMS measurements.

4. Conclusions

The detection limits for GDMS analyses of a number of impurities (B, Al, P, Ca, Ti, V, Cr, Mn, Fe, Ni, Co, Cu, Mo, Sn, W and Pb) of interest for solar cell applications have been investigated. These detection limits are approximately 1 ppba or below, except for B, Al, P Ca and Pb. All concentrations reported are quantitative since calculated RSF's for Si matrix have been used. The detection limits have been achieved with minimum sample preparation and short analysis time. These values are well below the level of impurities present in commercial silicon feedstock materials and, for most elements, below the level present in commercial crystalline silicon solar cells. GDMS is a valuable tool for quality- and contamination control in PV research and industry. The GDMS analyses of B in Si agree well with the SIMS analyses.

Acknowledgements

Thanks to NorSun (Norway) for providing the CZ-Si samples, Prof. Lars Arnberg (NTNU) and Dr. Joachim Hinrichs (Thermo Fisher Scientific) for scientific discussions. Ass. Prof. Lasse Vines (University of Oslo) is gratefully acknowledged for the SIMS analyses.

References

[1] J. Davis, A. Rothangi, H. Hopkins, D. Blais, P. Rai-Scoundhury, J.R. McCormick, C. Mollenkompf, Impurities in silicon solar cells, IEEE Electron Dev. Lett. 27 (1980) 677–687.

[2] A.A. Istratov, T. Buonassisi, M.D. Pickett, M. Heuer, E.R. Weber, Control of metal impurities in "dirty" multicrystalline silicon for solar cells, Mater. Sci. Eng. B 134 (2006) 282–286.
[3] R. Kvande, Incorporation of impurities during directional solidification of multicrystalline silicon for solar cells, PhD Thesis at NTNU, 2008.
[4] L.J. Geerligs, P. Manshanden, G.P. Wyers, E.J. Øvrelid, O.S. Raanes, A.N. Wærnes, B. Wiersma, Specification of solar grade silicon: how common impurities affect the cell efficiency of mc-Si solar cells, in: 20th EUPVSEC, 2005, pp. 619–622.
[5] L.J. Geerligs, P. Manshanden, I. Solheim, E.J. Øvrelid, A.N. Wærnes, Impact of common metallurgical impurities on mc-Si solar cell efficiency: p-type versus n-type doped ingots, in: 21st EUPVSEC, 2006, pp. 1285–1288.
[6] R. Kvande, L.J. Geerligs, G. Coletti, L. Arnberg, M. Di Sabatino, E.J. Øvrelid, C.C. Swanson, Distribution of iron in multicrystalline silicon ingots, J. Appl. Phys. 104 (2008).
[7] A.A. Istratov, T. Buonassisi, R.J. McDonald, A.R. Smit, R. Schindler, J.A. Rand, J.P. Kaleis, E.R. Weber, Metal content of multicrystalline silicon for solar cells and its impact on minority carrier diffusion length, J. Appl. Phys. 94 (2003) 6552–6559.
[8] D. Macdonald, A. Cuevas, A. Kinomura, Y. Nakano, Phosphorus gettering in multicrystalline silicon studied by neutron activation analysis, in: IEEE photovoltaic specialists, 2002, pp. 285–288.
[9] G. Coletti, Impurities in silicon and their impact on solar cell performance, PhD Thesis 2011, ISBN 978 9086 720 514.
[10] C. Modanese, M. Di Sabatino, A.K. Soiland, K. Peter, L. Arnberg, Investigation of bulk and solar cell properties of ingots cast from compensated solar grade silicon, Progr. PV 19 (2011) 45–53.
[11] M. Hystad, C. Modanese, M. Di Sabatino, L. Arnberg, Distribution and impact of Cr in compensated solar grade silicon, Sol. Energy Mater. Sol. Cells 103 (2012) 140–146.
[12] C. Modanese, M. Di Sabatino, A.K. Soiland, L. Arnberg, Relationship between net doping density and resistivity of compensated mc-Si ingots, Phisica Status Solidi 8 (2011) 713–716.
[13] S.W. Schmitt, C. Venzago, B. Hoffmann, V. Sivakov, T. Hofmann, J. Michler, S. Christiansen, G. Gamez, Glow glow discharge techniques in the chemical analysis of photovoltaic materials, Progr. Photovoltaics (2012), http://dx.doi.org/10.1002/pip.2264.
[14] ThermoFisher Scientific, Finnigan Element GD, Hardware Manual, 2005.
[15] M. Di Sabatino, A.L. Dons, J. Hinrichs, O. Lohne, L. Arnberg, Detection of trace elements in solar grade silicon by mass spectrometry, in: 22nd EUPVSEC, 2007.
[16] W.W. Harrison, C. Yang, E. Oxley, Mass spectrometry of glow discharges in Glow discharge plasmas in analytical spectroscopy, in: Marcus, Broekaert (Eds.), Wiley & Sons, 2003.
[17] M. Di Sabatino, A.L. Dons, J. Hinrichs, L. Arnberg, Determination of relative sensitivity factors for trace elements analysis of solar cell silicon by fast-flow glow discharge mass spectrometer, Spectrochim. Acta B 66 (2011) 144–148.
[18] M. Betti, Use of direct current glow discharge mass spectrometry for the chemical characterization of samples of nuclear concern, J. Anal. Atom. Spectrometry 11 (1996) 855–860.
[19] J. Hinrichs, M. Hamster, L. Rottmann, Analysis of solar cell silicon using glow discharge mass spectrometry, Application Note nr 30164, 2010.
[20] C. Modanese, L. Arnberg, M. Di Sabatino, Analysis of impurities with inhomogeneous distribution in multicrystalline solar cell silicon by glow discharge mass spectrometry, Mater. Sci. Eng. B 180 (2013) 27–32.